**ADVANCED
SCIENCE NEWS**

www.advancedsciencenews.com

**ADVANCED
MATERIALS**

www.advmat.de

COMMUNICATION

Toward Multispectral Imaging with Colloidal Metasurface Pixels

Jon W. Stewart, Gleb M. Akselrod, David R. Smith, and Maiken H. Mikkelsen*

Multispectral infrared (IR) imaging, an amalgamation of imaging and spectroscopy, is a critical tool for chemical and thermal sensing applications such as monitoring environmental pollutants,[1] detecting cancerous tissues,[2] and inspecting produce.[3] Despite the potential impact of multispectral technologies, its widespread usage has been significantly hindered by the complex scanning optical systems required. A promising approach to bypass this issue is to replace the scanning optical systems with multispectral focal plane arrays, composed of spectrally selective pixels.[4–7] However, the poor spectral selectivity of naturally occurring materials beyond the visible spectrum makes the fabrication of spectrally selective pixels exceedingly challenging.[8] Recently, metasurfaces consisting of subwavelength plasmonic resonators have demonstrated strong and spectrally selective absorption in the shortwave IR wavelengths,[6,8–10] promising for the realization of multispectral optoelectronics. However, to date plasmonic pixels or metasurfaces have been unable to simultaneously achieve narrow spectral selectivity, strong absorption, and scalable fabrication in the visible to near IR regimes. Here we demonstrate metasurface pixels exhibiting greater than 85% absorption and ≈100 nm spectral widths by patterning plasmonic resonators in micrometer-scale pixels using a fusion of bottom-up and top-down fabrication techniques over wafer-scale areas. The plasmonic resonators, tuned from 580 to 1125 nm, are composed of colloidally synthesized silver nanocubes separated from a gold film with a 4–10 nm spacer layer. To display the capability of this technique, we fabricate a multispectral metasurface pixel array consisting of six resonances and reconstruct a red, green, and blue (RGB) image with a combinatorial pixel scheme exhibiting 9261 color combinations.

Current plasmonic pixels in the visible to near IR regime have exhibited wide spectral ranges, nonfading colors, and have been demonstrated for a diverse set of applications ranging from photodetection to color printing.[11–25] However, the plasmonic resonators in this wavelength range have either poor absorption performance or broad spectral features due to their low quality factors, inherently limiting their applicability. Thus, plasmonic resonators with high absorption quality factors are desired to enable the construction of absorptive plasmonic pixels with narrower spectral features ideal for multispectral optoelectronic devices. A promising subwavelength element for constructing strongly absorbing, spectrally narrow pixels is the gap-plasmon resonator[12,14–17,19–24] due to its high field enhancements,[26–30] strong resonant modes,[31,32] and large electric and magnetic responsivities.[33–35] More specifically, plasmonic metasurfaces constructed with large surface area gap-plasmon resonators have shown many attractive optical properties including perfect absorption,[9,33–37] strong spectral selectivity,[5] and tunability anywhere from the ultraviolet (UV) to IR spectrum.[10,38] Thus, these metasurfaces are ideal candidates for integration into multispectral photodetectors, displays, and other optoelectronic devices.

The creation of multispectral optoelectronic devices based on plasmonic metasurfaces is contingent upon a fabrication method providing full control on multiple length scales. First, the plasmonic gap needs to be fabricated with nanometer accuracies in order to consistently control the plasmon resonance. Second, the subwavelength plasmonic resonators must be arranged spatially to form an impedance matched metasurface, resulting in perfect absorption on resonance. Third, these metasurfaces must be patterned on the micrometer scale into individual pixels forming multispectral arrays and finally the pixels must be patterned over wafer-scale areas to allow the fabrication of large-scale devices. To date, such plasmonic devices have yet to be demonstrated due to the lack of suitable fabrication methods with these multiscale properties. Traditional fabrication approaches, such as electron beam lithography or focused ion beam milling, can only achieve patterning resolutions on the order of tens of nanometers[9,11–13,17,22,23] and are not feasible for high-volume fabrication due to the slow write speeds and high cost. Other promising techniques for large-scale fabrication such as imprint lithography,[5,13–16,19] shadow evaporation,[27,39,40] among other approaches[41–43] have demonstrated control of plasmonic resonators down to 10 nm over large areas but lack single nanometer precision and may introduce other fabrication difficulties, e.g., associated with the incorporation of active materials into the plasmonic cavity. To bypass the limitations of these fabrication techniques, resonators can be fabricated through bottom-up colloidal assembly of film-coupled metallic nanoparticles, where the nanoparticles can be either cubes,[37] platelets,[44] disks,[34] or other geometries.[36,45,46] The accuracy of these vertically oriented gaps

J. W. Stewart, Dr. G. M. Akselrod, Prof. D. R. Smith,
Prof. M. H. Mikkelsen
Center for Metamaterials and Integrated Plasmonics
Duke University
Durham, NC 27708, USA
E-mail: m.mikkelsen@duke.edu
J. W. Stewart, Dr. G. M. Akselrod, Prof. D. R. Smith,
Prof. M. H. Mikkelsen
Department of Electrical and Computer Engineering
Duke University
Durham, NC 27708, USA
Prof. D. R. Smith, Prof. M. H. Mikkelsen
Department of Physics
Duke University
Durham, NC 27708, USA

depend upon the precision of the thin film deposition which can readily achieve subnanometer accuracies. On top of this, these vertical resonators can integrate a wide variety of materials in the gaps such as quantum dots,[47] 2D materials,[48] organic dyes,[49] and other materials deposited with atomic layer deposition.[50] The primary drawback of bottom-up assembly methods is that the spatial patterning of the metasurfaces into individual pixels cannot be controlled as needed for multispectral devices.

Here we demonstrate the creation of spectrally selective, highly absorbing metasurface pixels using a multiscale fabrication approach. This fabrication method utilizes a combination of bottom-up colloidal assembly to form the individual resonators and top-down photolithography to define the deposition of metasurfaces into multispectral patterns over multiple length scales. The only steps required for this process are dip coating, photolithography, and colloidal synthesis, which inherently make this fabrication method appealing for large-scale device fabrication. Leveraging this fabrication technique, two structures were fabricated demonstrating the unique capabilities of this plasmonic system. First, a wafer-scale multispectral metasurface pixel array was fabricated with six different resonances spanning from 580 to 1125 nm. Second, an RGB image was reconstructed in the near-IR with combinatorial metasurface pixels that achieve 9261 different color combinations.

The plasmonic metasurfaces are formed from colloidally synthesized metal nanocubes deposited on top of a metal film and separated by a polymer spacer with nanometer accuracies as shown in **Figure 1**. There are several appealing nanoscale properties of this plasmonic architecture. First, the plasmon resonance between the metal nanocubes and the film can be precisely controlled by varying the thickness of the gap layer, d, and the cube size, L, enabling the resonance to be tuned anywhere from 580 to 1420 nm.[37] Second, the gap size can be precisely maintained for individual particles across arbitrarily large samples through uniform coating techniques such as dip coating or atomic layer deposition. Furthermore, the effective properties of the surface can be tuned by varying the density of the nanocubes or by utilizing other plasmonic materials such as aluminum or silver.

A summary of the fabrication steps used to create the multispectral metasurfaces is illustrated in Figure 1, where the process utilizes colloidally synthesized silver nanocubes, layer-by-layer deposition of polyelectrolytes (PEs), and repeated lift-off photolithography. Initially, a gold film is evaporated on a silicon substrate (i) followed by spin coating of a negative photoresist (ii). Next, a photomask is used to determine the nanocube deposition area by exposing (iii) and developing (iv) the photoresist. A nanoscale spacer layer is then deposited using layer-by-layer dip coating of alternating PE layers composed of a positively charged poly(allylamine) hydrochloride (PAH) polymer and a negatively charged polystyrene sulfonate (PSS) polymer with layers of ≈1 nm thickness (v).[51] Next, the substrate is incubated in a solution of nanocubes (vi), where the nanocube stabilizer coating is polyvinylpyrrolidone (PVP), a negatively charged polymer, which facilitates the nanocubes to electrostatically adhere to the positively charged PE layer. The final film-nanocube separation distance is the sum of the PE layers and the 3 nm stabilizer coating. The silver nanocubes themselves
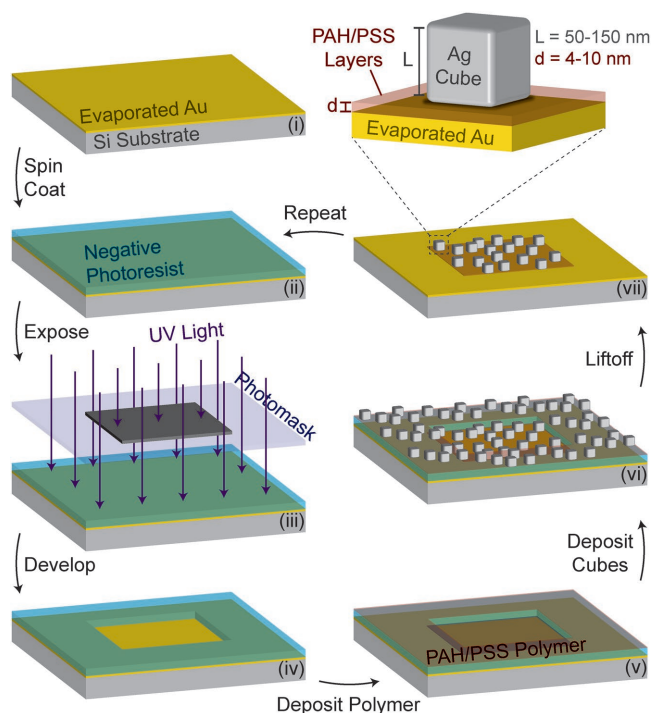

Figure 1. Fabrication procedure. Diagram illustrating the fabrication steps used to create multiple different self-assembled metasurface pixels on a single substrate. On the top right is a schematic of a single subwavelength absorber consisting of a silver nanocube separated from a gold substrate with a 4–10 nm polymer spacer layer.

are colloidally synthesized following a well-established process.[52,53] Lastly (vii), the photoresist is removed, leaving nanocubes only in the defined regions. The reflection spectra of the metasurfaces are essentially unaffected by the solvents used for the liftoff process as demonstrated in Figure S4 (Supporting Information). This fabrication process can be utilized to pattern any number of different nanocube resonances created with different gap thicknesses and nanocube sizes across large-scales by repeating the process starting with step (ii). The final result of this process is a sample with film-coupled plasmonic resonators with nanometer gap precisions, patterned into micrometer-scale pixels via photolithography over wafer-scale areas. This fabrication method can be extended to high-volume fabrication by automating the photolithography process with commercially available machines and by dip coating many substrates in parallel in polymer and nanocube baths.

Utilizing this method, a multispectral pixel array with six different metasurface resonances was patterned as illustrated in **Figure 2**. A photomask that consisted of 20 μm × 20 μm squares determined the locations of the nanocube deposition and the fabrication steps depicted in Figure 1 were repeated for each resonance. Resonances were chosen to vary from 580 to 1125 nm by using three different gap thicknesses, d, and three different sizes of nanocubes, L (Figure 2b). The scanning electron microscope (SEM) image in Figure 2a shows the uniform patterning of the multispectral pixel array over a small region of the full sample which covers a 1 cm × 1 cm area. The basic pixel unit of this structure is shown in Figure 2b where the cube sizes and gap thicknesses for each pixel are also indicated.

ADVANCED
SCIENCE NEWS
www.advancedsciencenews.com
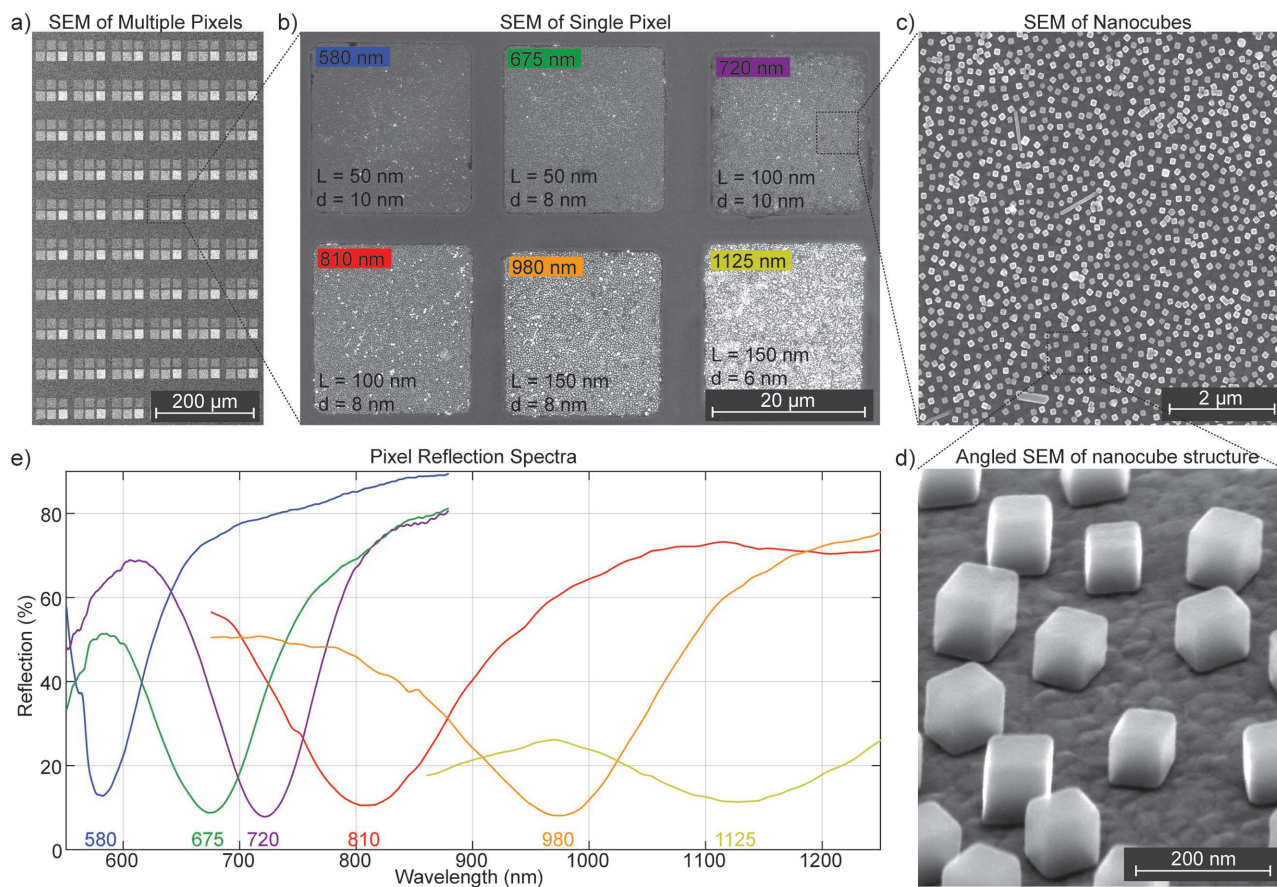
ADVANCED
MATERIALS
www.advmat.de

COMMUNICATION

Figure 2. Multispectral pixel array. a) SEM image of multiple pixels showing the uniformity of patterning. b) SEM image of a single pixel labeled according to their corresponding spectrums. The nanocube size, L, and the gap thickness, d, are labeled for each resonance. c) SEM image of the uniform distribution of cubes within the 20 μm × 20 μm squares. d) Angled SEM image showing silver nanocubes ($L = 75$ nm) on a gold substrate. e) Spectrum of six different plasmonic resonances across the visible to near infrared patterned on a single substrate.

The SEM image in Figure 2c shows that the metasurfaces are composed of an ensemble of randomly oriented nanocubes which also can be seen in an angled SEM in Figure 2d. The spectral response of each individual resonance was measured with a spectrometer with an integrated spot size of 5 μm in diameter and is shown in Figure 2e.

By fitting the spectra of each metasurface with a Lorentzian lineshape, the highest quality factors were determined to be 8.7 for the 580 nm resonant pixel and 6.3 for the 720 nm pixel. An analysis of the SEM image in Figure 2c reveals that 88% of the particles in the 720 nm metasurface were cubes with a ±6 nm size distribution as shown in Table S1 (Supporting Information). Figure S6 and Table S1 (Supporting Information) display the analysis results for the other metasurface pixels. The residual particles in the size distribution statistics are either clustered nanocubes, pyramids, rods, or other shapes. A peak absorption upward of 85% on resonance was achieved for each patterned metasurface. In this sample, the highest absorption peak of 90% occurs for the 720 nm resonance, which had the highest nanocube fraction of 88% with a ±6 nm size distribution that filled 16.1% of the surface area. The nanocube absorbers have previously demonstrated absorptions up to 99.7% at normal incidence and absorptions above 95% out to 50° angles of incidence using a solution consisting of 91%

nanocubes with a ±6 nm size distribution that filled 19.2% of the surface area.[37] The smaller peak absorptions observed in this work might be due to residual photoresist on the gold surface or interference of the photoresist walls with nanocube diffusion and adhesion causing the lower fill fractions exhibited here. While these factors potentially weaken the absorption performance of the metasurfaces, the performance could likely be improved with commercial photoresists or filtering the nanocube solutions to remove undesired larger particles.

Taking advantage of this multiscale fabrication technique, a second structure was designed that could reconstruct an arbitrary macroscopic RGB image through the use of combinatorial plasmonic pixels as depicted in **Figure 3**. Earlier plasmonic image reconstruction techniques have typically relied upon small variations in the plasmonic resonator to create up to 100 different colors with spatial resolutions up to ≈100 000 dots per inch (dpi).[11–18,20,21,23–25] Several recent approaches have demonstrated the capability of combinatorial plasmonic pixels to achieve a higher number of colors.[19,22] The multiscale fabrication technique presented here is uniquely suited to the creation of large-area plasmonic images reconstructed through the combination of multiple elemental colors with different intensities such as in RGB displays. The upper limit on the amount of colors is determined by the desired dpi and the accuracy with
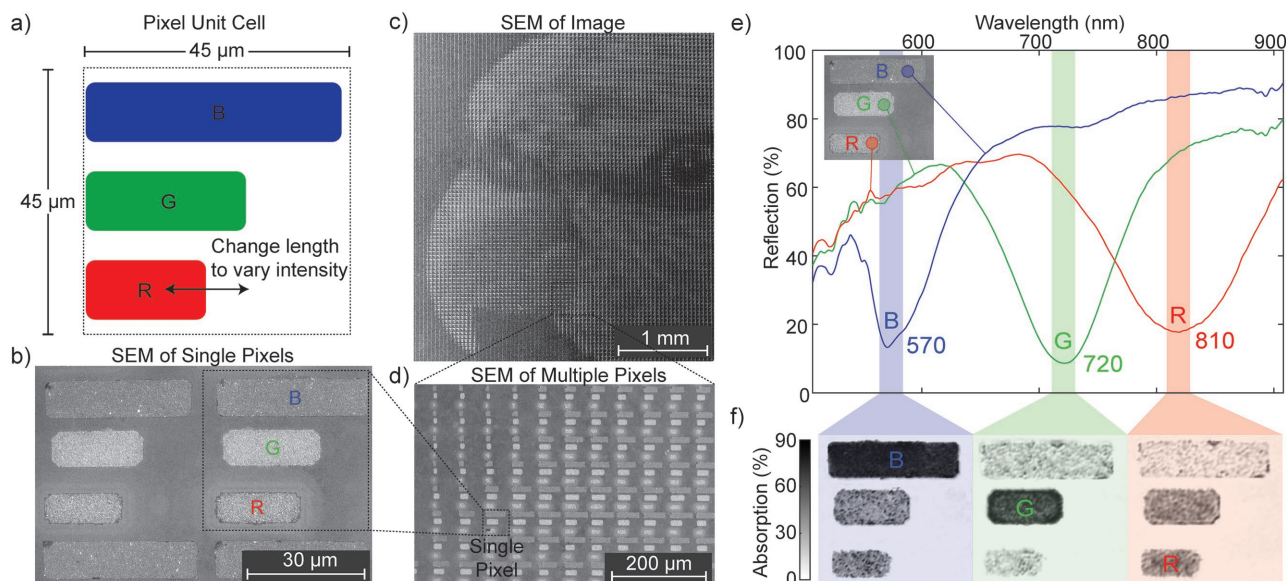
COMMUNICATION

Figure 3. Nanocube RGB pixel structure. a) Diagram of the pixel unit cell used to reconstruct an RGB image with the nanocube absorbers. The intensity of each color is tuned by varying the length of the rectangles in 2 µm increments. b) SEM image depicting actual pixels of the reconstructed RGB image. c) SEM image showing pixels with varying rectangle lengths along edge of parakeet head. d) SEM image of the parakeet head. e) Spectrum of three different colors used to reconstruct the RGB image. f) Images of pixels taken with ±10 nm bandpass filters around each resonance.

which the metasurfaces can be patterned. Here, each "RGB" pixel is mapped to a 45 µm × 45 µm square where the pixel color is changed by varying the length of a rectangular-shaped subpixel metasurface as depicted in Figure 3a. With 2 µm variations in length and a maximum length of 40 µm, each plasmonic subpixel can achieve 21 different absorption intensities for each color corresponding to 1% variations in the absorption of the R, G, or B channels which is easily measurable on commercial spectrometers. Thus with the 2 µm variations, this pixel scheme is readily capable of creating 9261 color combinations at a resolution of 560 dpi. An SEM image in Figure 3b shows pixels with varying "RGB" sizes that were fabricated. With this reconstruction method, each "RGB" channel can be mapped to any color between 570 and 1420 nm. In this specific case, the R channel was mapped to 810 nm, the G channel was mapped to 720 nm, and the B channel was mapped to 570 nm as shown in the spectrum of Figure 3e. Normalized microscope images of pixels were taken with ±10 nm bandpass filters around each resonance, shown in Figure 3f. The strong selectivity of the bandpass filters on the metasurfaces can be seen in the microscope images where the on-resonant pixels appear black.

An RGB image of a rainbow lorikeet was chosen to be reconstructed with the nanocube absorbers (**Figure 4**) and the image was down sampled from 256 intensities to the 21 intensities possible with the reconstruction method described above. Each pixel was then converted into three photomasks for the three different nanocube resonances needed. An SEM image demonstrating the variation of pixels along the edge of the lorikeet head is shown in Figure 3d. A macroscale SEM image in Figure 3c clearly shows how the lorikeet head is composed of individual three-color pixels. The sample was imaged with a custom built imaging system, in a white light reflection mode. The same bandpass filters used for Figure 3d were installed in front of the charge-coupled device (CCD) camera, and the images were

normalized for each different filter. Figure 4a shows images of the lorikeet in the separate color channels, with the images shown in false RGB color. The reconstructed image of the lorikeet head is shown in false color in Figure 4c with all three color channels. The image was reconstructed by resizing and superimposing the images to account for chromatic aberrations in the imaging system. The aliasing of the images is a result of slightly oversampling the image to where the individual pixel structures could be resolved. The original down-sampled image
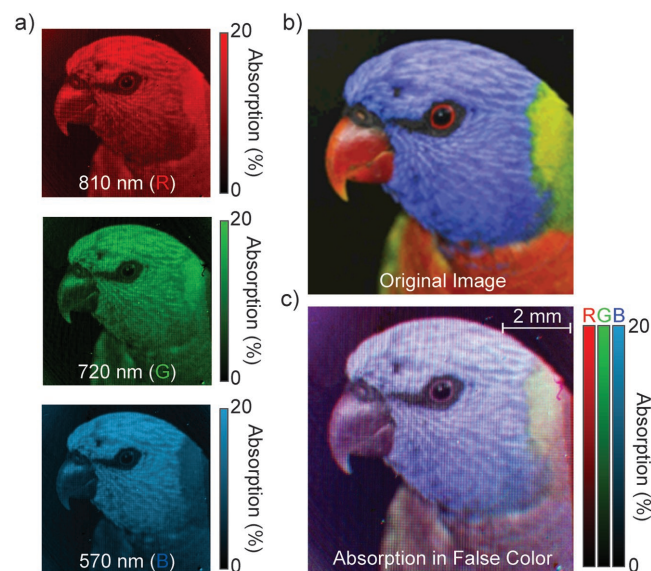

Figure 4. Reconstructed RGB image. a) Absorption images at the three different resonances taken with same bandpass filters as in Figure 3f. b) Original down-sampled image used to create the photomasks. c) The final reconstructed image from the three different absorption images.

is shown for comparison in Figure 4b. The red hue is observed to be less vibrant in the reconstructed metasurface image compared to the original, which is likely due to a slight degradation of the sample that occurred between fabrication and measurement. Typically, the PVP coating around the silver nanocubes protects them from oxidation for up to a week; however, the acetone liftoff used in the fabrication process affected the PVP coating resulting in faster degradation such as in the red pixels. The spectral effects of further oxidation on the sample can be seen in Figure S5 (Supporting Information). However, this image reconstruction is a clear visual demonstration of the precision with which the nanocube absorbers can be patterned on a macroscopic scale, with much finer features possible, limited only by the photolithography resolution.

This work demonstrated the creation of a large-scale multispectral metasurface pixel array and the reconstruction of a detailed macroscopic image through the use of a hybrid top-down, bottom-up fabrication approach. The resonance of the film-coupled resonators could be extended beyond the near-IR by utilizing colloidal nanocubes larger than 150 nm[54] or other large faceted nanoparticles. The patterning resolution could be significantly improved through the use of deep-UV lithography[55] promising for diffraction-limited plasmonic structures. Furthermore, the integration of bolometer-based photodetection schemes with the multispectral metasurface pixel arrays demonstrated here may be promising for the construction of multispectral image sensors. Similarly, semiconductor thin films could be inserted into the gap region of this nanocube structure to capture the hot electrons generated from the decay of the localized surface plasmons. Finally, thermally or electronically active materials could be integrated into the nanocube gap region for the creation of tunable, diffraction-limited plasmonic devices spanning from the visible to the mid-IR.

Experimental Section

Sample Preparation: The steps in this section will follow the outline provided in Figure 1. A smooth substrate, in this case a silicon wafer, was prepared and a thin metal film of 50–100 nm was deposited in step (i). In the samples presented, evaporated gold was used as the ground plane because of its low oxidation. The substrate used was a 5 mm p-type silicon wafer with 50 nm of gold and a 5 nm chromium adhesion layer deposited by electron beam evaporation. Initially, the gold substrate was oxygen etched in a reactive ion etcher (RIE) to remove organics from the surface. A negative photoresist, NFR016D2, was spun onto the sample with a thickness of ≈3 μm in step (ii). In step (iii), the photoresist was baked and then exposed with the desired photomask on a mask aligner. After baking again to develop the resist, it was etched with MF-319 to remove the unexposed areas in step (iv). The sample was then rinsed in DI water and dried. The sample was oxygen etched once again in the RIE to remove residual photoresist at the bottom of the unexposed areas. Next in step (v), cationic and anionic polymer layers were deposited. Both polymers were suspended in a one molar NaCl solution. The sample was alternately dip coated between the two ionic polymer suspensions and rinsed after each dip coating in a one molar NaCl solution to remove residual polymer. The sample was then rinsed with deionized (DI) water and dried. In step (vi), a nanocube solution was pipetted on top of the sample. A coverslip spacer was used to ensure uniform thickness of the solution over the sample and was kept in a refrigerator to reduce evaporation for 60 min. The silver nanocubes in this experiment were synthesized and provided by nanoComposix, Inc. in San Diego. The nanocube sizes varied between 50 and 140 nm

by controlling the parameters of the synthesis. In the last step (vii), the sample was sonicated in acetone for 10–30 s to remove the photoresist. The steps were repeated for each different resonance starting with step (ii), the spin coating of the photoresist.

Optical Measurements: The optical characterizations of the samples were carried out using a custom-made bright-field fluorescence microscope setup. A 20× magnification microscope objective was used for both the excitation and collection of reflected light. A pin-hole aperture is placed in the intermediate image plane to select light from certain areas of the sample. The white light reflectance measurements were conducted on this system at near normal incidence and were captured with a commercial spectrometer. The light source is a spectrally broad lamp emitting from the visible to the near-infrared regimes. The images of the pixels were collected using the same setup above with a 50× objective and a CCD camera. A diagram of the setup is shown in Figure S3 (Supporting Information).

The macroscopic reflectance images were captured using a custom-made reflection imaging setup. A 4f imaging system was constructed using a 1.2× stereoscope objective such that the white light is normally incident on the sample. Once again, a spectrally broad light source was used for the measurements. The reflected light collected from the objective was focused onto a CCD camera with an achromatic 4× objective lens. This allowed for the imaging of a 4.5 mm portion of the total 15 mm sample. Background images with no substrate and a gold substrate were used to extract the images of the sample independent of illumination intensity. The imaging setup is shown in Figure S2 (Supporting Information).

Supporting Information

Supporting Information is available from the Wiley Online Library or from the author.

[1] B. Zhang, D. Wu, L. Zhang, Q. Jiao, Q. L. Li, *Environ. Earth Sci.* **2012**, *65*, 649.

[2] H. Akbari, L. Halig, D. Schuster, A. Osunkoya, V. Master, P. Nieh, G. Chen, B. Fei, *J. Biomed. Opt.* **2012**, *17*, 0760051.

[3] A. A. Gowen, C. P. O'Donnell, P. J. Cullen, G. Downey, J. M. Frias, *Trends Food Sci. Tech.* **2007**, *18*, 590.

[4] J. Bao, M. Bawendi, *Nature* **2015**, *523*, 67.

[5] C. Wu, I. Neuner, G. Shvets, J. John, A. Milder, B. Zollars, S. Savoy, *Phys. Rev. B* **2011**, *84*, 075102.

[6] W.-Y. Jang, Z. Ku, A. Urbas, J. Derov, M. Noyola, *IEEE Trans. Geosci. Remote* **2015**, *53*, 3471.

[7] S. Lee, S. Krishna, S. Brueck, *IEEE Photonics Technol. Lett.* **2011**, *23*, 935.

[8] J. Talghader, A. Gawarikar, R. Shea, *Light Sci. Appl.* **2012**, *1*, e24.

[9] N. Liu, M. Mesch, T. Weiss, M. Hentschel, H. Giessen, *Nano Lett.* **2010**, *10*, 2342.

[10] A. Tittl, A. K. Michel, M. Schäferling, X. Yin, B. Gholipour, L. Cui, M. Wuttig, T. Taubner, F. Neubrech, H. Giessen, *Adv. Mater.* **2015**, *27*, 4597.

[11] J. Olson, A. Manjavacas, L. Liu, W.-S. Chang, B. Foerster, N. King, M. Knight, P. Nordlander, N. Halas, S. Link, *Proc. Natl. Acad. Sci. USA* **2014**, *111*, 14348.

[12] M. Miyata, H. Hatada, J. Takahara, *Nano Lett.* **2016**, *16*, 3166.

[13] J. Olson, A. Manjavacas, T. Basu, D. Huang, A. Schlather, B. Zheng, N. Halas, P. Nordlander, S. Link, *ACS Nano* **2015**, *10*, 1108.

[14] J. Clausen, E. Højlund-Nielsen, A. Christiansen, S. Yazdi, M. Grajower, H. Taha, U. Levy, A. Kristensen, N. Mortensen, *Nano Lett.* **2014**, *14*, 4499.

[15] X. Zhu, C. Vannahme, E. Højlund-Nielsen, A. N. Mortensen, A. Kristensen, *Nat. Nanotechnol.* **2015**, *11*, 325.

[16] K. Kumar, H. Duan, R. Hegde, S. Koh, J. Wei, J. Yang, *Nat. Nanotechnol.* **2012**, *7*, 557.

[17] X. Goh, Y. Zheng, S. Tan, L. Zhang, K. Kumar, C.-W. Qiu, J. Yang, *Nat. Commun.* **2014**, *5*, 5361.

[18] J. Henzie, M. Lee, T. Odom, *Nat. Nanotechnol.* **2007**, *2*, 549.

[19] T. James, P. Mulvaney, A. Roberts, *Nano Lett.* **2016**, *16*, 3817.

[20] L. Wang, R. Ng, S. Dinachali, M. Jalali, Y. Yu, J. Yang, *ACS Photonics* **2016**, *3*, 627.

[21] R. Yu, P. Mazumder, N. Borrelli, A. Carrilero, D. Ghosh, R. Maniyara, D. Baker, F. Abajo, V. Pruneri, *ACS Photonics* **2016**, *3*, 1194.

[22] S. Tan, L. Zhang, D. Zhu, X. Goh, Y. Wang, K. Kumar, C.-W. Qiu, J. Yang, *Nano Lett.* **2014**, *14*, 4023.

[23] T. Chen, B. M. Reinhard, *Adv. Mater.* **2016**, *28*, 3522.

[24] Y. Gu, L. Zhang, J. Yang, S. Yeo, C.-W. Qiu, *Nanoscale* **2015**, *7*, 6409.

[25] Q. Chen, X. Hu, L. Wen, Y. Yu, D. Cumming, *Small* **2016**, *12*, 4922.

[26] S. Maier, *Opt. Express* **2006**, *14*, 1957.

[27] T. Siegfried, Y. Ekinci, O. Martin, H. Sigg, *Nano Lett.* **2013**, *13*, 5449.

[28] C. Ciracì, R. Hill, J. Mock, Y. Urzhumov, A. Fernández-Domínguez, S. Maier, J. Pendry, A. Chilkoti, D. R. Smith, *Science* **2012**, *337*, 1072.

[29] A. Rose, T. Hoang, F. McGuire, J. Mock, C. Ciracì, D. Smith, M. Mikkelsen, *Nano Lett.* **2014**, *14*, 4797.

[30] J. Schuller, E. Barnard, W. Cai, Y. Jun, J. White, M. Brongersma, *Nat. Mater.* **2010**, *9*, 193.

[31] O. Hess, J. Pendry, S. Maier, R. Oulton, J. Hamm, K. Tsakmakidis, *Nat. Mater.* **2012**, *11*, 573.

[32] Q. Bai, M. Perrin, C. Sauvan, J.-P. Hugonin, P. Lalanne, *Opt. Express* **2013**, *21*, 27371.

[33] A. Moreau, C. Ciracì, J. Mock, R. Hill, Q. Wang, B. Wiley, A. Chilkoti, D. R. Smith, *Nature* **2012**, *492*, 86.

[34] R. Walter, A. Tittl, A. Berrier, F. Sterl, T. Weiss, H. Giessen, *Adv. Opt. Mater.* **2015**, *3*, 398.

[35] A. Tittl, P. Mai, R. Taubert, D. Dregely, N. Liu, H. Giessen, *Nano Lett.* **2011**, *11*, 4366.

[36] Z. Fang, Y.-R. Zhen, L. Fan, X. Zhu, P. Nordlander, *Phys. Rev. B* **2012**, *85*, 245401.

[37] G. M. Akselrod, J. Huang, T. B. Hoang, P. T. Bowen, L. Su, D. R. Smith, M. H. Mikkelsen, *Adv. Mater.* **2015**, *27*, 8028.

[38] M. Knight, N. King, L. Liu, H. Everitt, P. Nordlander, N. Halas, *ACS Nano* **2014**, *8*, 834.

[39] M. Zhang, N. Large, A. Koh, Y. Cao, A. Manjavacas, R. Sinclair, P. Nordlander, S. Wang, *ACS Nano* **2015**, *9*, 9331.

[40] T. Siegfried, Y. Ekinci, H. Solak, O. Martin, H. Sigg, *Appl. Phys. Lett.* **2011**, *99*, 263302.

[41] Z.-K. K. Zhou, J. Xue, Z. Zheng, J. Li, Y. Ke, Y. Yu, J.-B. B. Han, W. Xie, S. Deng, H. Chen, X. Wang, *Nanoscale* **2015**, *7*, 15392.

[42] A. Dhawan, Y. Du, D. Batchelor, H. N. Wang, D. Leonard, V. Misra, M. Ozturk, M. Gerhold, T. Vo Dinh, *Small* **2011**, *7*, 727.

[43] H. Im, K. Bantz, N. Lindquist, C. Haynes, S.-H. Oh, *Nano Lett.* **2010**, *10*, 2231.

[44] J. Hao, J. Wang, X. Liu, W. Padilla, L. Zhou, M. Qiu, *Appl. Phys. Lett.* **2010**, *96*, 251104.

[45] F. Cheng, X. Yang, J. Gao, *Opt. Lett.* **2014**, *39*, 3185.

[46] Y. Avitzour, Y. Urzhumov, G. Shvets, *Phys. Rev. B* **2009**, *79*, 045131.

[47] T. B. Hoang, G. M. Akselrod, C. Argyropoulos, J. Huang, D. R. Smith, M. H. Mikkelsen, *Nat. Commun.* **2015**, *6*, 7788.

[48] J. Huang, T. Hoang, M. Mikkelsen, *Sci. Rep.* **2016**, *6*, 22414.

[49] G. M. Akselrod, C. Argyropoulos, T. B. Hoang, C. Ciracì, C. Fang, J. Huang, D. R. Smith, M. H. Mikkelsen, *Nat. Photonics* **2014**, *8*, 835.

[50] J. Lassiter, X. Chen, X. Liu, C. Ciracì, T. B. Hoang, S. Larouche, S.-H. Oh, M. H. Mikkelsen, D. R. Smith, *ACS Photonics* **2014**, *1*, 1212.

[51] J. Mock, R. Hill, A. Degiron, S. Zauscher, A. Chilkoti, D. R. Smith, *Nano Lett.* **2008**, *8*, 2245.

[52] Y. Wang, Y. Zheng, C. Huang, Y. Xia, *J. Am. Chem. Soc.* **2013**, *135*, 1941.

[53] T. B. Hoang, J. Huang, M. H. Mikkelsen, *J. Visualized Exp.* **2016**, *111*, e53876.

[54] Q. Zhang, W. Li, C. Moran, J. Zeng, J. Chen, L.-P. Wen, Y. Xia, *J. Am. Chem. Soc.* **2010**, *132*, 11372.

[55] Q.-Y. Lin, Z. Li, K. Brown, M. O'Brien, M. Ross, Y. Zhou, S. Butun, P.-C. Chen, G. Schatz, V. Dravid, K. Aydin, C. Mirkin, *Nano Lett.* **2015**, *15*, 4699.